Dual Energy CT Attenuation Correction Methods for Quantitative Assessment of Response to Cancer Therapy with PET/CT Imaging.

Paul E. Kinahan[1], Adam M. Alessio[1], Jeffrey A. Fessler[2]

[1]Department of Radiology, University of Washington
[2]Department of Electrical Engineering and Computer Science, University of Michigan

Abstract

We hypothesize that improved quantification for PET imaging of high atomic number materials can be achieved by combining low-dose x-ray imaging with dual energy CT for PET attenuation correction. Improved quantification of tracer uptake will lead to improved patient outcomes by providing more accurate information for therapeutic choices. Accurate PET/CT measurements of early response will be critical in determining the best cancer therapy option for each patient in a timely manner and in sparing patients the morbidity and cost of ineffective treatments. We first evaluate the potential errors in PET images arising from CT-based attenuation correction when iodine-based contrast is incorrectly classified as bone when forming the linear attenuation coefficient image. We then investigate two methods of reducing errors in the linear attenuation image: an approximate, but fast, hybrid classification/scaling algorithm and a model-based dual-energy CT method that incorporates the polyenergetic spectrum and a noise model in an iterative reconstruction method. Both methods are shown to reduce errors in the estimated linear attenuation coefficient image, but require further study to determine the effects of noise propagation if low-dose CT scans are used for the estimation of the linear attenuation image.

INTRODUCTION

Positron emission tomography (PET) radiotracer imaging with the labeled glucose analog 18F-fluorodeoxyglucose (FDG) is being used increasingly in oncology imaging due to its usefulness in detecting and staging cancer and metastatic disease (1-4). A promising application of PET is tumor imaging with newly developed tracers for therapy monitoring with proliferation and apoptosis markers and definition of the tumor environment throughout therapy, constituting a strong basis for an individually tailored therapy for tumor patients (5-9).
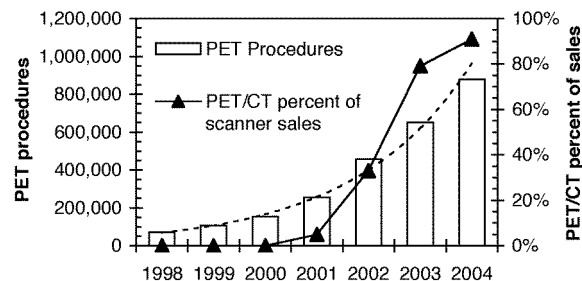

Fig.1. Number of PET procedures per year. The dotted line is an exponential fit ($r^2 = 0.99$) indicating a doubling time of 19 months. Roughly 90% of PET procedures are oncology studies. Also shown is the percentage of new PET or PET/CT scanner sales that are PET/CT scanners (right axis). The total number of PET and PET/CT scanner sales has also been rising: 342 in 2001, 417 in 2002, and 450 in 2003. Data compiled from (12-15).

The advent of the dual modality PET/CT scanner (10) has significantly enhanced the physician's armamentarium for the diagnosis and staging of cancer as well as for therapy planning and monitoring response to therapy. PET/CT has become the most comprehensive diagnostic tool in oncology imaging by providing improved lesion identification and localization (11). Estimates of

the numbers of FDG PET scans performed in the U.S. are shown in Fig. 1, which also indicates the rapid saturation by PET/CT systems of the new PET scanner sales market.

The primary purpose of combining CT and PET systems in a single scanner is the precise anatomical localization of regions identified on the PET tracer uptake images (16, 17). Although it is possible to use non-rigid image registration to align separately-acquired whole-body PET and CT images, challenges remain in the practical implementation and validation of software-based methods (18, 19).

Identifying Early Response to Cancer Therapy

A widely used standard for monitoring the effect of cancer therapy on solid tumors is the evaluation of size changes measured from CT images. The Response Evaluation Criteria in Solid Tumors (RECIST) standard specifies a 'positive response' as a 30% decrease in the maximum diameter. This approach has several problems, including the long time lag after therapy (six months or more) necessary for anatomical changes to become evident. By then if there is no response, time may have run out for other treatment options for the patient. In addition the patient may have undergone several months of ineffective but toxic therapy. Furthermore, cytostatic agents, such as the lung cancer drug erlotinib, inhibit tumor growth when successful but may not lead to cell death and reduction in tumor size, in which case tumor size is not a good measure of response. While RECIST guidelines provide an important standard for evaluating response, alternative and robust methods of evaluating response by biochemical imaging are needed to improve patient management especially with increasing therapeutic choices.
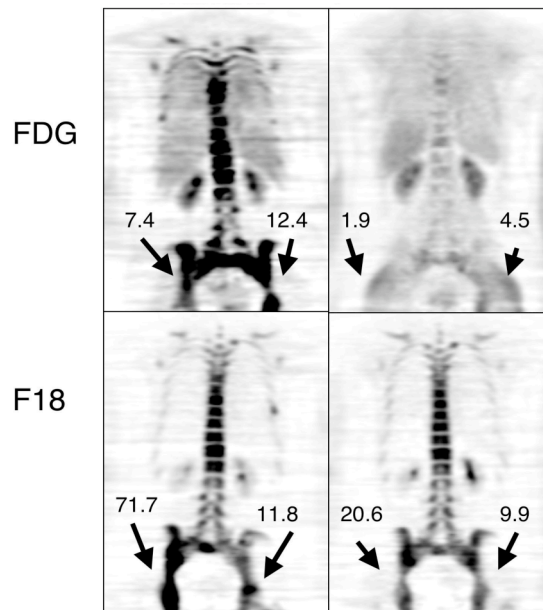

Fig. 2. Change in glucose metabolism and fluoride incorporation in bone-dominant metastatic breast cancer. These images demonstrate glucose metabolism (FDG) and bone fluoride incorporation (F18) in a patient with widespread bony metastases from breast cancer before (left) and after hormonal therapy (right). Numbers shown are standardized uptake values (SUVs), a measure of relative tracer uptake. Data courtesy of Dr. David Mankoff, University of Washington.

There has been increasing awareness of the value of identifying early response to cancer therapy. On January 10th, 2005, the National Cancer Institute (NCI) sponsored a "Workshop on the Role of FDG-PET in the Evaluation of Therapeutic Response in Cancer". One of the conclusions from the workshop was that improved quantification is needed, including robust and accurate methods for PET/CT. Fig. 2 illustrates the use of PET imaging to assess response to

therapy. The images demonstrate an excellent response to therapy, which had been underestimated by conventional imaging modalities, including CT and bone scans. Some notable features are: The distribution of bony abnormalities is different between FDG PET and fluoride PET. Response to therapy is qualitatively and quantitatively apparent in the FDG PET image. The qualitative appearance of the fluoride image, however is relatively stable over the course of treatment, and response to therapy is based largely on quantitative assessment. This emphasizes the need for accurate quantification.

<u>CT-based attenuation correction (CTAC)</u>

An important synergy of PET/CT scanners is the use of the CT images for attenuation correction of the PET emission data (20-22). All manufacturers of PET/CT scanners incorporate X-ray CT based attenuation correction (CTAC) algorithms in their systems, and for the majority of PET/CT scanners it is the only option offered (23). This approach offers the significant advantage that the CT data has much lower statistical noise and can be acquired in a shorter time than a standard PET transmission scan (20). CT transmission scans can also be acquired after the PET tracer is injected, allowing the ability to collect unbiased post-injection transmission scans. This reduces image bias from emission contamination while shortening the time spent by a patient on the scanner bed and providing more efficient use of scanner time.

To be used for attenuation correction, the CT data must be transformed to an estimate of the attenuation coefficients at 511 keV. However, there is no unique transformation from CT energies (~30 to 140 keV) to 511 keV due to the possibility of independent variations in density and atomic number (Z) (24). Two materials with different atomic numbers may have similar CT values but different attenuation coefficients at 511 keV. Conversely, it is possible for two distinct materials with the same value of attenuation coefficient at 511 keV to have different CT numbers.

Biases in the CTAC image propagate to errors in the PET image in the same general location (25). Three methods have been considered for converting a CT image to attenuation coefficients at 511 keV: segmentation, scaling, and dual-energy X-ray scans.

Segmentation: Methods can be used to separate the CT image into regions corresponding to different tissue types, which are then replaced with appropriate attenuation coefficients at 511 keV. However, some tissue and bone regions have continuously-varying densities that cannot be accurately represented by a discrete set of segmented values (26). The increased noise of low-dose CTAC scans can result in misclassification of voxels, with incorrect attenuation coefficients being assigned. For these reasons, segmentation methods have not been adopted for CTAC transforms, although they may have some application for the correction of focal accumulations of CT contrast agents (27, 28).

Scaling: It is possible to estimate the attenuation map of the patient at 511 keV simply by multiplying the entire CT image by the ratio of attenuation coefficients of water (representing soft tissues) at the photon energies of CT and PET. For bone, however, linear scaling is a poor approximation, since photoelectric absorption dominates Compton scatter at the lower range of CT energies (29). Blankespoor et al. (30) used bilinear scaling to convert CT images to 140 keV for attenuation correction of SPECT data. In this method, different scaling factors (for water and air, and for water and bone respectively) are used to calculate the attenuation values for CT numbers H for which -1000 < H < 0, and for H > 0. The bilinear scaling method has been shown to give reasonable results for low-Z biological materials in practice (21, 31, 32). For high-Z materials such as contrast agents there is some disagreement in the literature. Some investigators report no significant errors introduced by high-Z materials when using scaling methods (33), while others have measured quantitative errors (28, 34-38). While in many cases

any CTAC errors may not significantly affect diagnostic utility, they may affect decisions or therapies that depend on accurate estimation of tracer uptake in response to therapy.

The errors introduced by high-Z materials can be understood from Fig. 3, which illustrates the standard bilinear method used for estimating the linear attenuation coefficient ($\mu(x,y)$ (cm-1)) image at 511 keV from the CT image. Each voxel in the CT image is scaled according to the "bilinear" transform, which has different slopes for air/water and water/bone mixtures, as described above (22). For iodine, the transformation that *should* be used is illustrated, but unfortunately there is no way to discriminate iodine from bone based on the CT voxel value alone. Thus either voxels containing contrast are incorrectly scaled as bone, or if the iodine curve is used to produce correct results for contrast agent, then voxels containing bone are incorrectly scaled as contrast agent.
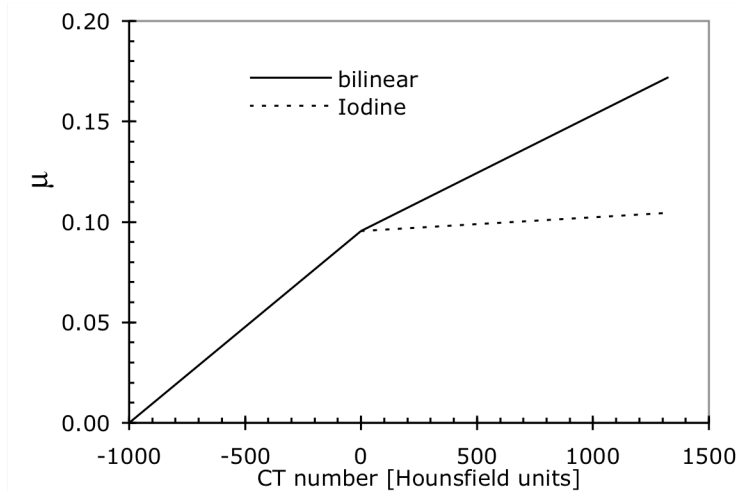

Fig. 3. Bilinear scaling factors used to convert CT numbers to linear attenuation coefficients at 511 keV. Also show is the transformation that *should* be used for iodine-based contrast agents.

Dual Energy X-ray Imaging: A quantitatively accurate estimate of the linear attenuation coefficients at 511 keV can be obtained by collecting two CT scans using X-ray beams with different energy spectra and by estimating the energy dependence of attenuation coefficients in terms of a Compton scattering component and a photoelectric absorption component (39, 40), or by other material bases. The separate component images can then be combined to synthesize an accurate image of attenuation coefficients at any energy. Numerous medical applications of dual-energy imaging, such as bone mineral density measurements (41), as well as non-medical applications have been explored (42). Dual-energy CTAC would allow for accurate attenuation correction in PET/CT imaging that involves high-Z materials, including bone, contrast, and metals. This approach was used to form a mono-energetic attenuation map at 140 keV by Hasegawa et al. for a prototype SPECT/CT detector block (43) and for separate SPECT and CT scans by Guy et al. (44). A drawback of the dual-energy CT method is that the inverse problem of estimating the component sinograms is poorly conditioned (45), leading to excessive noise amplification. To make dual-energy CTAC feasible for PET/CT imaging, additional steps are needed to reduce noise in the estimated attenuation image at 511 keV. Image reconstruction algorithms that model the acquisition physics can reduce statistical noise in DECT. There have, however, been very few iterative image reconstruction algorithms proposed for DECT. Sukovic and Clinthorne have investigated iterative algorithms for dual-energy CT reconstruction based on a weighted least-squares approach assuming *monoenergetic* scans (46). We describe below a *polyenergetic* version of the Sukovic and Clinthorne weighted least-squares algorithm for CTAC estimation appropriate for PET/CT

scanners (47, 48), and evaluate its usefulness for dual energy CTAC. We call this method the dual-energy weighted least-squares algorithm (DE-WLS).

We also investigate an approximate dual-energy method (called hybrid DECTAC) that allows discrimination of contrast from bone (49, 50). This allows the selection of correct scaling factors for bone versus contrast, but not necessarily other materials. Recently Bacharach et al described the same approach (51). Watson et al described a related method (52) that used dual-energy CT to correctly estimate bone linear attenuation values.

We first evaluate the potential errors in PET images arising from CT-based attenuation correction when contrast is incorrectly classified as bone in the estimation of the linear attenuation coefficient image. We then investigate the two methods described above for reducing errors in the linear attenuation image: the approximate, but fast, hybrid classification/scaling algorithm and the model-based dual-energy CT method that incorporates the polyenergetic spectrum and a noise model in an iterative reconstruction method.

MATERIALS AND METHODS

Impact of Errors from Contrast Agent Enhancement

We first investigate the bias introduced by incorrect estimation of linear attenuation coefficients estimated by the standard bi-linear method. This used computer simulations of a abdomen-sized object with a set of six test objects (5 cm diameter regions) of differing standardized uptake values (SUVs) with two different local background SUVs as illustrated in fig. 4(left). The two background regions had SUVs of 1.0 and 2.0, while the test objects had SUVs of 0.5, 1.0, 2.0, and 3.0 as shown. The corresponding attenuation values for the six objects should ideally have the linear attenuation coefficient as background. We simulated the effect of contrast agent being incorrectly scaled as bone, as illustrated in fig. 4(right). The effect of contrast agent enhancement of 20, 100, and 500 Hounsfield unites (HU) were evaluated for each SUV of the test objects.
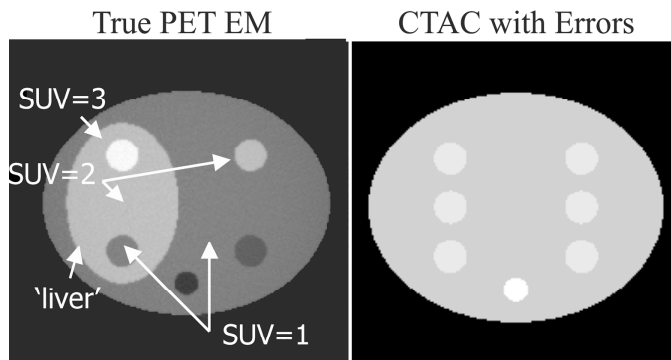

Fig 4. Test objects used for simulation study investigating the propagation of errors from biased attenuation correction factors (CTAC with errors) into the attenuation corrected PET image.

Method 1: Hybrid Dual-Energy CTAC (DECTAC)

The proposed dual-energy hybrid method classifies materials based on their changes in CT number from scans at two different kVp, taking advantage of the large differences in the photoelectric cross-sections of iodine and barium versus calcium (53) to determine how to scale each voxel in the CTAC image.

Since bone and contrast values span a wide range of CT values, we have derived a classification scheme for the CT difference images e.g. (80 and 140 kVp) by simply using the

mid-point of the relative change in CT numbers, in other words the HU difference depends on the HU value to account for variable concentrations of contrast and variable bone density (fig. 5) (49). When the correct material (bone or contrast) is determined, then the appropriate scaling factor from fig. 3 is applied to the corresponding voxel in the first CT image.
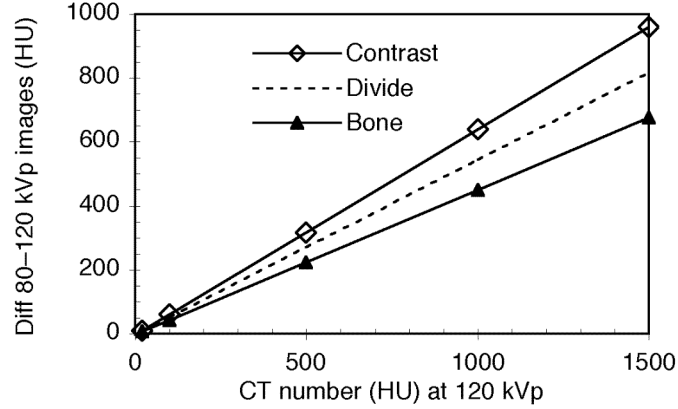

Fig. 5. DE-CTAC Classification scheme. Contrast versus bone discrimination is accomplished by determining if the change in CT number is greater than a threshold, which depends on the CT number for one of the kVp images.

To test this approach, we acquired CT measurements at 80, 100, 120, and 140 kVp of a 20 cm diameter test phantom containing water and 5 cm diameter cylinders of air, dilute iodine-based contrast agent and $CaCl_2$ in solution (bone equivalent atomic number). The resulting CT numbers were evaluated at each tube voltage. The standard bilinear CT scaling method and the hybrid method were applied to the 140 kVp CT image. A standard PET transmission scan was also acquired for reference.

Method 2: Dual-Energy Weighted Least-squares Algorithm (DE-WLS)

The above Hybrid DE-CTAC hybrid scheme will help discriminate contrast from bone, but will not suffice if unknown or multiple high-Z materials are present. We have implemented a new PWLS algorithm for dual energy CT similar to that of Sukovic and Clinthorne (46), but with a polyenergetic model of the spectrum, rather than their monoenergetic approach (47, 48). We term this the dual-energy weighted least-squares (DE-WLS) algorithm. To derive the algorithm we start with a parameterization that uses basis functions that are each separable in space and energy $\mu(\vec{x}, E) = \sum_{l=1,L} \sum_{j=1,N_P} \beta_l(E) b_j(\vec{x}) x_{lj}$, where $\beta_l(E)$ is the mass attenuation of the lth material type, $b_j(\vec{x})$ are spatial basis functions, and x_{lj} are the desired coefficients for material l and voxel j. Thus the spatially-varying density of each material is given by $\rho_l(\vec{x}) = \sum_j b_j(\vec{x}) x_{lj}$ and the system model is given by $a_{ij} = \int_{L_i} b_j(\vec{x}) d\ell$, where L_i denotes the ith line of response (LOR). The material basis sinograms are then given by $s_{il}(\mathbf{x}_l) \triangleq \int_{L_i} \rho_l(\vec{x}) d\ell = \sum_{i=1,N_p} a_{ij} x_{lj}$. To solve for $\mathbf{x}$, we use the PWLS criterion: $\mathbf{x} = \arg\min \Psi(\mathbf{x})$, with $\Psi(\mathbf{x}) \triangleq \sum_{i=1}^{N_D} (\hat{\mathbf{s}}_i - \mathbf{s}_i(\mathbf{x}))' \mathbf{W}_i (\hat{\mathbf{s}}_i - \mathbf{s}_i(\mathbf{x})) + R(\mathbf{x})$, where N_D is the number of lines of response, and $\hat{\mathbf{s}}_i$ are the material basis sinograms estimated from the CT sinograms using standard dual-energy decomposition methods, and $\mathbf{W}_i$ are the inverse variances of $\hat{\mathbf{s}}_i$. The function R(x) is a regularizer that controls noise.

We tested the DE-WLS approach with simulated and measured data. For the simulations we used a 20 cm diameter phantom containing three smaller 5 cm diameter cylinders comprised of (1) air, (2) half soft tissue and half bone with a total density of 1.5 g/cm^3; and (3) a bone cylinder

with a total density of 2g/cm^3. The large background cylinder was all soft tissue component with a density of 1 g/cm^3. The attenuation coefficients at 511 keV were estimated by (1) standard bilinear scaling, (2) dual energy CT with a standard dual-energy decomposition method followed by filtered backprojection (FBP) and the DE-WLS algorithm.

RESULTS

Impact of Errors from Contrast Agent Enhancement

Fig. 6 illustrates the effects of biases from CT-based attenuation correction for noiseless PET simulations. The difference image between the true PET image (fig. 4) and the reconstructed image is also shown. The errors, expressed as standardized uptake values (SUV), are plotted in fig. 7 as a function of the SUV of the test object for the different levels of contrast-induced CT number errors.

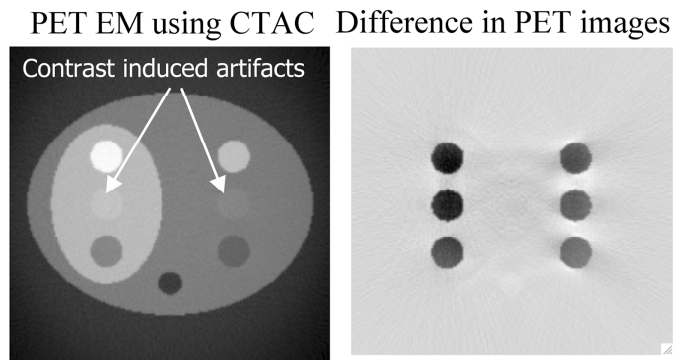PET EM using CTAC   Difference in PET images

Figure 6. Noiseless simulation study showing propagation of errors from biased attenuation correction factors into the attenuation corrected PET image (PET EM using CTAC). A difference image from the true PET image (fig. 4) shows that both quantitative errors and complex artifacts can occur.
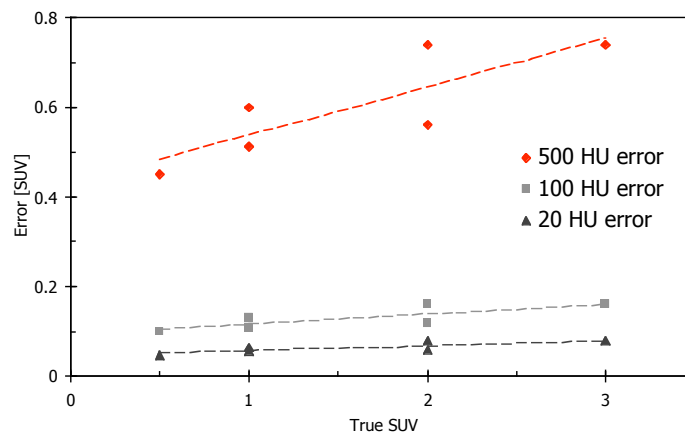

Fig 7. Results of simulation study showing propagation of CT error of different Hounsfield units (HU) into the error in the attenuation corrected PET standard uptake values (SUV).

Method 1: Hybrid Dual-Energy CTAC (DECTAC)

For the measured phantom data there was essentially no variation in CT number for air or water with tube voltage. For the CaCl$_2$ solution the CT numbers increased from 546 to 897 HU, while the dilute contrast agent values increased from 856 to 1721 HU as the tube voltage was

dropped from 140 to 80 kVp. Thus, starting from a standard CT scan at 120 kVp, a second (low-dose) CT scan at 80 kVp would show a difference of ~400 HU between contrast agents and CaCl2 (bone equivalent). This is similar to heuristic bone-imaging procedures for CT. One of the dual-energy difference images is shown in fig. 8, which shows that there is no variation in CT number with kVp for both air and water, while there are differing variations for bone and contrast agent. The difference image is sensitive to the photoelectric absorption, which is higher in iodine-based contrast agent than in bone.
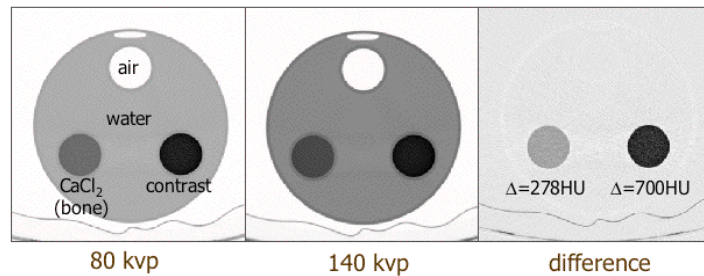

Fig. 8. Measured 20 cm diameter water cylinder with 5 cm cylindrical inserts containing air, bone-equivalent solution of CaCl2 and dilute iodine-based contrast agent scanned at 2 different kVp.

By classifying the voxels in the CT image (fig. 8) based on the scheme illustrated in fig. 5, the correct scaling factors for bone and contrast agent (fig. 3) can be used to convert the CT image to an estimate of the linear attenuation coefficients at 511 keV. This was evaluated as shown in fig. 9 for the same test phantom used in fig. 8. The bilinear method has a substantial error for the 5 cm diam. contrast agent filled region, when compared to the measured PET transmission scan at 511 keV. This error is reduced from -38% to + 6% with the use of the dual energy hybrid/bilinear method.
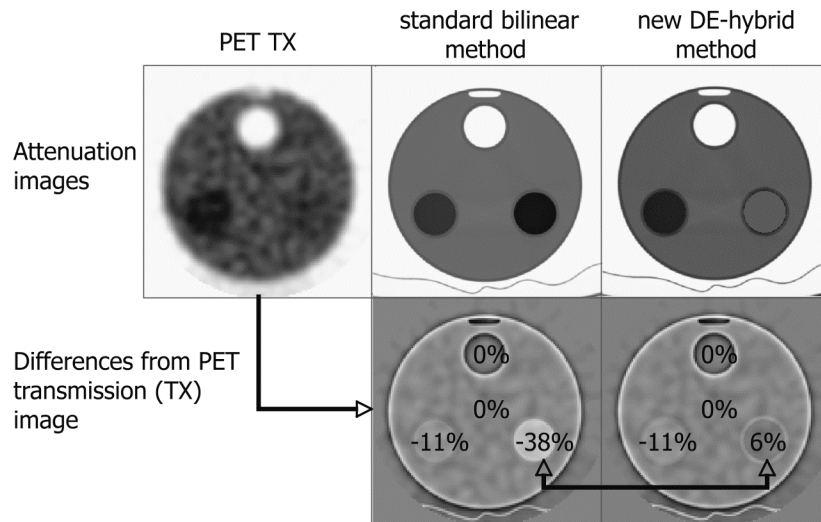

Fig. 9. Effect of bilinear and hybrid scaling methods on measured data, compared to measured PET transmission scan (TX).

Method 2: Dual-Energy Weighted Least-squares Algorithm (DE-WLS)

Results of the simulation studies are shown in Fig. 10. The CT-based attenuation images were scaled to 511 keV by either bilinear scaling or dual energy CT. The dual-energy CT images were reconstructed with both FBP and the DE-WLS algorithms. Also shown (bottom) are the differences from the true values at 511 keV. There is a significant reduction of bias using DECT

(from 20% to ~0% for the tissue/bone mixture) compared to bilinear scaling. The FBP image, however, has high levels of statistical noise, as expected. These noise levels are reduced from ~8% to ~3% by the use of our DE-WLS algorithm. Within the object RMS errors decrease from 11% using bi-linear scaling to 9% with DE-FBP and to 7.5% with DE-WLS.

↓Differences with true attenuation image at 511 keV

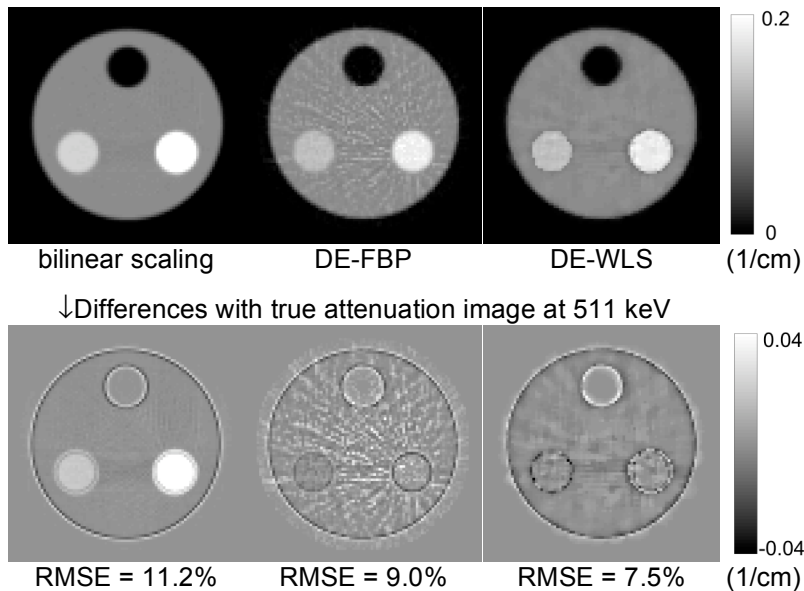RMSE = 11.2%   RMSE = 9.0%   RMSE = 7.5%   (1/cm)

Fig. 10. Comparison of CT-based attenuation images scaled to 511 keV by either bilinear scaling or dual energy CT. Also shown (bottom row) are the differences from the true values at 511 keV.

The computation time of the DE-WLS (with 10 iterations) and FBP methods are shown in fig. 11 for a standard workstation. There is a significant increase in computation time required for the DE-WLS, which would render it infeasible for clinical implementation with standard 512x512 CT images. For attenuation correction of PET data, however, only 128x128 (or perhaps even 64x64) images are needed, for relatively thick slices, which reduces the DE-WLS computation time down to clinically feasible levels.
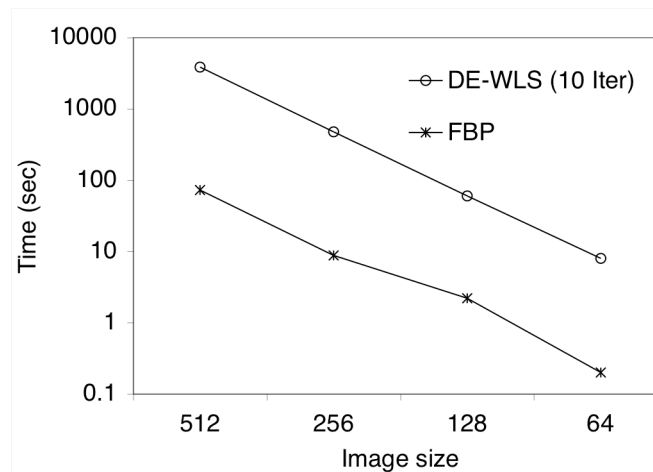

Fig. 11. Computation time for the DE-WLS and FBP algorithms as a function of image size when implemented on a standard workstation.

DISCUSSION

Currently, CT attenuation correction has the potential for significant bias in the attenuation correction factors. We present results showing the propagation of these errors into attenuation corrected PET images. Dual energy CT-based attenuation correction offers the potential of reducing bias in the CTAC image and thus can also reduce bias in the final PET emission image.

Dual energy CT attenuation correction results in increased noise in reconstructions from the basis material decomposition process and from the potential use of low-dose CT. Noise from dual energy CT imaging can be reduced through the use of: (1) a statistically principled reconstruction method, (2) a coarse reconstruction grid, and (3) only the summed component image at 511keV.

Both the simulated and measured phantom results demonstrate the feasibility of using dual-energy CTAC for accurate attenuation correction in PET/CT oncology imaging. We have shown that with the dual-energy hybrid method it is possible to discriminate contrast versus bone in the CTAC images and apply the correct scale factor for accurate calibration and attenuation correction. We note that this method may not be suitable for standard 512 x 512 high resolution CT images due to patient motion or noise amplification. However, for low-resolution 128 x 128 (or even 64 x 64) CTAC images reconstructed with statistically-principled algorithms we expect that the noise amplification will be acceptable.

We also evaluated a polychromatic DE-PWLS iterative reconstruction method that is potentially more accurate than the dual-energy hybrid method. We showed that the reduction of the CTAC sinograms and image matrix sizes to 128×128 or 64×64 leads to iterative reconstructions of dual energy CT component images in a clinically feasible amount of time.

In addition to errors from scaling the CTAC image to 511 keV described above, three other sources of error from CT-based attenuation have been recognized (10, 22): CT field of view truncation artifacts, CT beam hardening, and respiratory motion mismatch between the PET and CT acquisitions. An ameliorating factor for truncation artifacts is that missing attenuation correction factors can be closely approximated from the truncated projection data, leading to accurate CTAC images (54). We also note that beam hardening effects are minimized by the use of a dual energy CT method. Research in compensating for respiratory motion are ongoing.

Conclusion

We presented two successful DECT strategies for reducing quantitative errors from CT-based attenuation correction. The quantitative biases present in PET/CT imaging clearly do not prevent its effective use in the diagnosis and staging of cancer. However, a key component of the use of PET in the management of cancer will be for evaluating response to therapy and for making therapeutic choices. These applications require the use of quantitative PET/CT imaging to assure they have a positive impact on patient management. Accurate PET/CT measurements of early response will be critical in determining the best cancer therapy option for each patient in a timely manner and in sparing patients the morbidity and cost of ineffective treatments.

REFERENCES

1. Wahl RL. Clinical Oncology Update: The emerging role of positron emission tomography: Part I. Principal and Practice of Oncology Updates. 1997;11:1-18.
2. Weber WA, Avril N, Schwaiger M. Relevance of positron emission tomography (PET) in oncology. Strahlentherapie und Onkologie. 1999;175:356-373.
3. Bomanji JB, Costa DC, Ell PJ. Clinical role of positron emission tomography in oncology. Lancet Oncology. 2001;2:157-164.
4. Rohren EM, Turkington TG, Coleman RE. Clinical applications of PET in oncology. Radiology. 2004;231:305-332.
5. Krohn KA, Mankoff DA, Eary JF. Imaging cellular proliferation as a measure of response to therapy. Journal of Clinical Pharmacology. 2001;Suppl:96S-103S.
6. Mankoff DA, Muzi M, Krohn KA. Quantitative positron emission tomography imaging to measure tumor response to therapy: what is the best method? Molecular Imaging & Biology. 2003;5:281-285.
7. Cohade C, Wahl RL. PET scanning and measuring the impact of treatment. Cancer J. 2002;8:119-134.
8. Stahl A, Wieder H, Piert M, Wester HJ, Senekowitsch-Schmidtke R, Schwaiger M. Positron emission tomography as a tool for translational research in oncology. Molecular Imaging in Biology. 2004;6:214-224.
9. Juweid ME, Cheson BD. Positron-emission tomography and assessment of cancer therapy. N Engl J Med. 2006;354:496-507.
10. Beyer T, Townsend DW, Brun T, et al. A combined PET/CT scanner for clinical oncology. Journal of Nuclear Medicine. 2000;41:1369-1379.
11. Czernin J. Summary of selected PET/CT abstracts from the 2003 Society of Nuclear Medicine Annual Meeting. Journal of Nuclear Medicine. 2004;45:102S-103S.
12. Burns M. PET market appears poised for continued strong growth. Diagnostic Imaging. 2003
13. Ridley EL. PET/CT growth sparks gains in U.S. PET market. AuntMinniecom. 2003
14. Staff. PET usage surges in 2002. AuntMinniecom. 2003
15. Staff. PET procedure volume to surge. AuntMinniecom. 2004
16. Wahl RL, Quint LE, Cieslak RD, Aisen AM, Koeppe RA, Meyer CR. "Anatometabolic" tumor imaging: fusion of FDG PET with CT or MRI to localize foci of increased activity. J Nucl Med. 1993;34:1190-1197.
17. Townsend DW, Beyer T, Blodgett TM. PET/CT scanners: a hardware approach to image fusion. Semin Nucl Med. 2003;33:193-204.
18. Slomka PJ. Software approach to merging molecular with anatomic information. J Nucl Med. 2004;45 Suppl 1:36S-45S.
19. Wahl RL. Why nearly all PET of abdominal and pelvic cancers will be performed as PET/CT. Journal of Nuclear Medicine. 2004;45:82S-95S.
20. Kinahan PE, Townsend DW, Beyer T, Sashin D. Attenuation correction for a combined 3D PET/CT scanner. Med Phys. 1998;25:2046-2053.
21. Burger C, Goerres G, Schoenes S, Buck A, Lonn AH, Von Schulthess GK. PET attenuation coefficients from CT images: experimental evaluation of the transformation of CT into PET 511-keV attenuation coefficients. Eur J Nucl Med Mol Imaging. 2002;29:922-927.

22. Kinahan PE, Hasegawa BH, Beyer T. X-ray Based Attenuation Correction for PET/CT Scanners. Seminars in Nuclear Medicine. 2003;33:166-179.

23. Alessio A, Kinahan PE, Cheng P, Vesselle H, Karp JS. PET/CT Scanner Instrumentation, Challenges, and Solutions. Radiologic Clinics of North America. 2004;42:1017-1032.

24. Schneider W, Bortfeld T, Schlegel W. Correlation between CT numbers and tissue parameters needed for Monte Carlo simulations of clinical dose distributions. Physics in Medicine and Biology. 2000;45:459-478.

25. Bai CY, Kinahan PE, Brasse D, et al. An analytic study of the effects of attenuation on tumor detection in whole-body PET oncology imaging. Journal of Nuclear Medicine. 2003;44:1855-1861.

26. Robinson PJ, Kreel L. Pulmonary tissue attenuation with computed tomography: comparison of inspiration and expiration scans. Journal of Computer Assisted Tomography. 1979;3:740-748.

27. editors. CT-Based Attenuation Correction for PET/CT Scanners in the Presence of Contrast Agent. 2002; Norfolk, VA: IEEE; 2002.

28. Nehmeh SA, Erdi YE, Kalaigian H, et al. Correction for oral contrast artifacts in CT attenuation-corrected PET images obtained by combined PET/CT. Journal of Nuclear Medicine. 2003;44:1940-1944.

29. LaCroix KJ, Tsui BMW, Hasegawa BH, Brown JK. Investigation of the use of X-ray CT images for attenuation compensation in SPECT. IEEE Transactions on Nuclear Science. 1994;NS-41:2793-2799.

30. Blankespoor SC, Wu X, Kalki JK, et al. Attenuation Correction of SPECT Using X-Ray CT on an Emission-Transmission CT System: Myocardial Perfusion Assessment. IEEE Transactions on Nuclear Science. 1996;43:2263-2274.

31. Kamel E, Hany TF, Burger C, et al. CT vs 68Ge attenuation correction in a combined PET/CT system: evaluation of the effect of lowering the CT tube current. Eur J Nucl Med Mol Imaging. 2002;29:346-350.

32. Nakamoto Y, Osman M, Cohade C, et al. PET/CT: comparison of quantitative tracer uptake between germanium and CT transmission attenuation-corrected images. J Nucl Med. 2002;43:1137-1143.

33. Dizendorf E, Hany TF, Buck A, von Schulthess GK, Burger C. Cause and magnitude of the error induced by oral CT contrast agent in CT-based attenuation correction of PET emission studies. Journal of Nuclear Medicine. 2003;44:732-738.

34. Antoch G, Jentzen W, Freudenberg LS, et al. Effect of oral contrast agents on computed tomography-based positron emission tomography attenuation correction in dual-modality positron emission tomography/computed tomography imaging. Investigative Radiology. 2003;38:784-789.

35. Bujenovic S, Mannting F, Chakrabarti R, Ladnier D. Artifactual 2-deoxy-2-[(18)F]fluoro-D-glucose localization surrounding metallic objects in a PET/CT scanner using CT-based attenuation correction. Mol Imaging Biol. 2003;5:20-22.

36. Goerres GW, Ziegler SI, Burger C, von Schulthess T, Buck A. Artifacts at PET and PET/CT caused by metallic hip prosthetic material. Radiology. 2003;226:577-584.

37. Nakamoto Y, Chin BB, Kraitchman DL, Lawler LP, Marshall LT, Wahl RL. Effects of nonionic intravenous contrast agents at PET/CT imaging: Phantom and canine studies. Radiology. 2003;227:817-824.

38. Visvikis D, Costa DC, Croasdale I, et al. CT-based attenuation correction in the calculation of semi-quantitative indices of F-18 FDG uptake in PET. European Journal of Nuclear Medicine and Molecular Imaging. 2003;30:344-353.

39. Alvarez R, Seppi E. Comparison of Noise and Dose in Conventional and Energy Selective Computed-Tomography. IEEE Transactions on Nuclear Science. 1979;26:2853-2855.

40. Alvarez RE, Macovski A. Energy-Selective Reconstructions in X-Ray Computerized Tomography. Physics in Medicine and Biology. 1976;21:733-744.

41. Greenfield MA. Current status of physical measurements of the skeleton. Medical Physics. 1992;19:1349-1357.

42. Engler P, Friedman WD. Review of Dual-Energy Computed-Tomography Techniques. Materials Evaluation. 1990;48:623-629.

43. Hasegawa BH, Lang TF, Brown EL, et al. Object specific attenuation correction of SPECT with correlated dual-energy X-ray CT. IEEE Transactions on Nuclear Science. 1993;NS-40:1242-1252.

44. Guy MJ, Castellano-Smith IA, Flower MA, Flux GD, Ott RJ, Visvikis D. DETECT - Dual energy transmission estimation CT - for improved attenuation correction in SPECT and PET. IEEE Transactions on Nuclear Science. 1998;45:1261-1267.

45. Kalender WA, Klotz E, Kostaridou L. An Algorithm for Noise Suppression in Dual Energy CT Material Density Images. Ieee Transactions on Medical Imaging. 1988;7:218-224.

46. Sukovic P, Clinthorne NH. Penalized weighted least-squares image reconstruction for dual energy X-ray transmission tomography. Ieee Transactions on Medical Imaging. 2000;19:1075-1081.

47. Sonka M, Fitzpatrick JM, editors. Maximum-likelihood dual-energy tomographic image reconstruction. 4684(1); 2002; San Diego, CA, USA: SPIE; 2002.

48. editors. Quantitative attenuation correction for PET/CT using iterative reconstruction of low-dose dual-energy CT. 5; 2004; 2004.

49. editors. Dual-Energy CT For Quantitative Attenuation Correction In PET/CT Imaging. 2004; Chicago, IL: 2004.

50. Kinahan PE, Alessio AM, Fessler JA, Lewellen TK, Vesselle H. A Simple Dual Energy Method for CT-Based Attenuation Correction That Accounts for Contrast Agents in PET/CT Imaging. Journal of Nuclear Medicine. 2005;46:113P(abstract).

51. Bacharach SL, Freedman NMT, Maass-Moreno R, Le Meunier L. Dual Energy CT for Detecting Contrast Media in PET/CT. Journal of Nuclear Medicine. 2005;46(5):168P (abstract).

52. Watson CC, Rappoport V, Faul D, Townsend DW, Carney JP. A method for calibrating the CT-based attenuation correction of PET in human tissue. Nuclear Science, IEEE Transactions on Nuclear Science, IEEE Transactions on. 2006;53:102-107.

53. Hubbell JH, Seltzer SM. Tables of X-Ray Mass Attenuation Coefficients and Mass Energy-Absorption Coefficients. 1997;January, 2003

54. editors. Algorithm to Extend Reconstruction Field-of-View. 2004; Arlington, VA: IEEE; 2004.